
# IrO2-incorporated La0.8Sr0.2MnO3 as bifunctional oxygen electrocatalysts with enhanced activities

| | |
|---|---|
| Journal: | *Inorganic Chemistry Frontiers* |
| Manuscript ID | QI-RES-01-2019-000033.R1 |
| Article Type: | Research Article |
| Date Submitted by the Author: | 01-Mar-2019 |
| Complete List of Authors: | Wang, Haizhen; New Mexico State University<br>Yan, Litao; New Mexico State University<br>Nakotte, Tom; New Mexico State University<br>Xu, Weichuan; New Mexico State University College of Agricultural Consumer and Environmental Sciences,<br>Zhou, Meng; New Mexico State University<br>Ding, Dong; Idaho National Laboratory, Energy & Environment Science and Technology<br>Luo, Hongmei; New Mexico State University |
| | |

# $IrO_2$-incorporated $La_{0.8}Sr_{0.2}MnO_3$ as bifunctional oxygen electrocatalysts with enhanced activities

Haizhen Wang,[1] Litao Yan,[1] Tom Nakotte,[1] Weichuan Xu,[1] Meng Zhou,[1] Dong Ding,[2,*] and Hongmei Luo[1,*]

[1] Department of Chemical and Materials Engineering, New Mexico State University, Las Cruces, NM 88003, United Stated.

[2] Energy & Environment Science and Technology, Idaho National Laboratory, Idaho Falls, ID 83415, United States.

*Corresponding authors. E-mails: hluo@nmsu.edu (HL) and dong.ding@inl.gov (DD).

**Abstract:** Developing low-cost and highly efficient oxygen electrocatalysts for both oxygen evolution reaction (OER) and oxygen reduction reaction (ORR) has become one important issue recently due to the sluggish kinetics of these two reactions, which requires high overpotentials thus high energy input. Perovskite oxides have emerged as a new class of highly efficient non-precious metal catalysts for oxygen electrocatalysis in alkaline media. In this work, $IrO_2$-incorporated $La_{0.8}Sr_{0.2}MnO_3$ composite has been developed as a novel bifunctional oxygen electrocatalyst using polymer-assisted approach with subsequent wet impregnation-calcination method. Due to the synergistic effect between the high ORR activity of $La_{0.8}Sr_{0.2}MnO_3$ and the good OER activity of $IrO_2$ as well as the improved electrochemically active surface area, the electrocatalytic activities of the composite for both OER and ORR has been improved, compared with the pristine $La_{0.8}Sr_{0.2}MnO_3$ ($\Delta E$=1.043 V), resulting in its enhanced bifunctionality ($\Delta E$=0.652 V) as oxygen catalysts in alkaline solution, which is also superior to the reported state-of-the-art electrocatalysts. The stability test shows that after 1000 cycles of cyclic voltammetry (CV), there is only 15 mV positive shift for achieving a current density of 10 mA $cm^{-2}$ in OER and 17 mV negative shift to reach a current density of -1 mA $cm^{-2}$ of ORR, which indicates the good stability of the electrocatalyst (5 wt% $IrO_2$ incorporated $La_{0.8}Sr_{0.2}MnO_3$) in alkaline solution. Our study not only reports a new composite material as a bifunctional oxygen electrocatalyst, but also opens a new avenue to develop novel perovskite oxide-based electrocatalysts with enhanced bifunctional electrocatalytic activities.

**Keywords:** $IrO_2$-incorporated, $La_{0.8}Sr_{0.2}MnO_3$, synergistic effect, bifunctional, oxygen catalysts

## 1. Introduction

Increasing energy depletion of fossil fuels caused by economic development and the related human activities has caused more and more extensive research on developing innovative electrochemical energy storage and conversion devices, such as metal-air batteries[1] and alkaline fuel cells,[2, 3] which are capable of storing and converting electrical energy with much improved efficiency and low cost. The performance of these devices is dominantly governed by two oxygen electrocatalysis reactions in alkaline solutions, oxygen reduction reaction (ORR) at the cathode and oxygen evolution reaction (OER) at the anode. However, due to the sluggish kinetics of these reactions,[4] the development or even commercialization of those electrochemical devices are still hindered even though catalysts have been introduced in order to reduce the overpotential of these reactions. The most active catalyst for ORR is Pt-based materials.[5-7] However, they are not active for OER since the formation of Pt oxide on the surface[8] at high potentials blocks their catalytic ability for OER. On the contrary, $IrO_2$ has been reported as the most active catalyst for the OER[9, 10] due to its good electrical and ionic conductivities, but not effective for ORR. Besides, both Pt and $IrO_2$-based materials belong to noble-metals which are very expensive[2-4] and show poor activity[11] during operation, prohibiting their large-scale applications. Therefore, development of alternative highly efficient non-noble metal catalysts with earth-abundant low-cost elements and bifunctionality for both ORR and OER is desperately required to replace the precious metal catalysts, which remain a challenge to widespread application of these electrochemical energy technologies.

Different materials, including transition metal oxides[11, 12], carbon-based materials[13, 14] with flexible structures have been extensively demonstrated as potential electrocatalysts for OER and ORR. However, carbon-based materials are not as stable as metal oxides, especially under oxidative environments.[3] Thus, more and more research has been focused on non-noble metal

oxides development, especially mixed metal oxides, including spinel and perovskite oxides, since multiple redox-active metal ions can buffer the multi-electron process necessary for water oxidation.[15] Among the metal oxides, perovskites are known as promising and competitive bifunctional catalysts for both ORR and OER, due to their high ionic/electronic conductivity, electrochemical stability as well as low cost.[3, 16] Perovskites with a formula of $ABO_3$, in which A sites are usually rare-earth or alkali metal ions and B sites are mostly transition metal ions, are composed of $BO_6$ octahedra with A-site cations at the corner of the unit cell. This unique structure allows them to accommodate wide range of metal ions.[17] Besides, their physi-chemical and catalytic properties can also be flexibly tuned through A/B site substitution or doping in a wide composition ranges,[15, 17] which render them with a new formula of $A_aA'_{1-a}B_bB'_{1-b}O_{3-x}$ and exhibit intrinsic activities comparable to those precious metal-based catalysts.

Perovskites have been first proposed to be oxygen electrocatalysts in 1970,[18] which was followed by subsequent wide exploration of different kinds of perovskite oxides for oxygen electrocatalytic behavior studies. Until now, several strategies have been developed to improve the electrocatalytic performance of perovskite oxides as oxygen electrocatalyst for either OER or ORR or even both reactions. Some researchers have introduced deficiency[19, 20] or doping[21] with new metal ions in A-site of perovskites, resulting in oxygen vacancy inside perovskites while other researchers have doped metal ions into the B-site[11, 22, 23] of perovskite oxides to provide extra redox active sites. Besides, different perovskites with various particle size/morphology [21, 24] also have been synthesized with increased surface area and thus more active sites would be exposed to the catalytic reactions. Furthermore, another promising approach also has been contemplated recently through the incorporation of two metal oxides[25-28] with different electrocatalytic activities for OER and ORR, especially combination of noble metal oxides with non-noble metal oxides[29, 30] to

develop efficient composite electrocatalysts. It is widely accepted that the synergistic effect between the two metal oxides results in the enhanced electrocatalytic behavior.

Manganite perovskites have been reported to exhibit high activity[4, 16, 31] for ORR among perovskite oxides but have low intrinsic activity for OER while $IrO_2$ is highly active OER catalyst with low activity for ORR. In this paper, we aim at increasing the electrocatalytic performance of $La_{0.8}Sr_{0.2}MnO_3$ for both OER and ORR via incorporation of $IrO_2$. First, $La_{0.8}Sr_{0.2}MnO_3$ was synthesized using polymer-assisted approach[11, 32] and $IrO_2$ was introduced via wet impregnation-calcination method. The electrochemical measurements in alkaline electrolyte indicate that $IrO_2$-incorporated $La_{0.8}Sr_{0.2}MnO_3$ exhibit better electrochemical catalytic performance for both OER and ORR compared with pristine $La_{0.8}Sr_{0.2}MnO_3$, resulting in improved bifunctionality as oxygen catalysts. To the best of our knowledge, it is the first time that we report the combination of $IrO_2$ with $La_{0.8}Sr_{0.2}MnO_3$ perovskites produces a synergistic bifunctional catalytic effect for both OER and ORR, which opens a new avenue to design new catalyst system based on the perovskite oxides with enhanced bifunctional electrocatalytic behavior.

## 2. Experimental section

### 2.1 Materials

Poly(ethylenimine) (PEI) (50 % w/v in $H_2O$), ethylenediaminetetraacetic acid (EDTA) (> 99.4 %), lanthanum nitrate ($La(NO_3)_3 \cdot 6H_2O$, 99.99 %), strontium nitrate ($Sr(NO_3)_2$, 99.995 %), manganese acetate tetrahydrate ($Mn(Ac)_2 \cdot 4H_2O$, >99 %), iridium trichloride hydrate ($IrCl_3 \cdot xH_2O$), potassium hydroxide (KOH) and ammonium hydroxide solution (ACS reagent, 28.0-30.0 % $NH_3$ basis) were purchased from Sigma-Aldrich. All chemicals were used as received without further purification.

### 2.2 Synthesis of $La_{0.8}Sr_{0.2}MnO_3$ (denoted as LSM)

The synthetic process is the same as reported previously by our group.[4] In detail, 2 g PEI and 1 g EDTA was dissolved in certain amount of deionized water to form a clear transparent metal-

polymer complex solution. Then 0.8 mmol $La(NO_3)_3 \cdot 6H_2O$, 0.2 mmol $Sr(NO_3)_2$ and 1 mmol $Mn(Ac)_2 \cdot 4H_2O$ powders were added to the previous polymer precursor solution sequentially, which was further stirred for another 2 h until the powders were dissolved. Then the resultant solution was transferred to a crucible which was placed into a furnace. The furnace was set to a temperature of 650 $^oC$ with a ramp rate of 1 $^oC$/min, which was kept at 650 $^oC$ for 3 h. LSM powder was collected when the furnace cooled down to room temperature.

2.3 Synthesis of $IrO_2$-incorporated $La_{0.8}Sr_{0.2}MnO_3$

Certain amount of $IrCl_3 \cdot xH_2O$ was dissolved in deionized water and stirred until dissolved to form a light-yellow solution. Then 50 mg LSM powder was added to the solution (ammonium hydroxide solution was used to adjust the pH value to be around 11). The solution was further stirred for 24 h and transferred to a crucible which was heated to 500 $^oC$ with a ramp rate of 1 $^oC$/min and kept in 500 $^oC$ for 4 h. The samples of 5 wt% $IrO_2$-incorporated $La_{0.8}Sr_{0.2}MnO_3$ and 10 wt% $IrO_2$-$La_{0.8}Sr_{0.2}MnO_3$ are denoted as LSMI5 and LSMI10, respectively. 5 wt% refers that $IrO_2$ occupies about five weight percent with reference to the total amount of LSM based on the original $IrCl_3 \cdot xH_2O$ added to the precursor solution, assuming that all $IrCl_3 \cdot xH_2O$ could be converted to $IrO_2$.

2.4 Characterization

The structure and the composition of the samples were examined using X-ray diffraction (XRD). XRD was performed using a PANalytical Empyrean powder diffractometer with Cu Ka (λ=1.5406 Å) at 45 kV and 40 mA. The particle size and the morphology of the materials was examined with transmission electron microscopy (TEM) on H-7650 instrument, (Hitachi High-Technologies Corp), which was analyzed at a voltage of 80 kV. The $N_2$ adsorption and desorption measurement was used to study the surface areas of the samples by the Brunauer-Emmett-Teller (BET) method with a Micromeritics ASAP 2050 instrument operated at 77 K. X-ray photoelectron spectroscopy

(XPS) was used to investigate the surface composition of the samples, which was executed on a Thermo K-Alpha spectrometer equipped with a monochromatic Al kα X-ray source. Energy dispersive X-ray spectroscopy (EDS) with elemental mapping was used to examine the surface elemental composition, which was tested in a scanning electron microscopy (SEM) S-3400 N with incorporated energy dispersive x-ray microanalysis system (Noran system six 300, Thermo Electron Corp). High resolution TEM (HRTEM) was conducted on JEOL 3000 F with high resolution imaging. TGA test was performed on a thermogravimetric analyzer (TGA-Q500, TA Instruments, New Castle, DE) using platinum pans under $O_2$ atmosphere with a heating rate of 10 $^oC$/min to 900 $^oC$.

2.5 Electrochemical measurements

The electrocatalytic measurements were studied using a standard three-electrode electrochemical cell with a rotating disk connected to a potentiostat instrument (CHI 760C) in a 0.1 mol $L^{-1}$ KOH solution at room temperature. The three-electrode cell consists of platinum (Pt) coil as the counter electrode, Ag(s)|AgCl(s) (3.5 mol $L^{-1}$ KCl) as reference electrode and the products loaded on the glassy carbon as the working electrode. A KCl agar–agar salt bridge was used between the cell and the reference electrode. The as-prepared metal oxide powder (5 mg) was dispersed in 1 mL $H_2O$ with 0.05 wt % diluted Nafion®117 solution to form the catalyst ink and sonicated for around 30 mins while no conductive carbon/acetylene black was mixed with the catalyst, which is different from other reported work.[33] Since it has been reported that there is thin layer of carbon coating remaining on the surface of the perovskites due to the incomplete decomposition of polymer when the metal-polymer precursor solution is heated at lower temperature.[31, 34] Further, the existence of carbon in the as-prepared $La_{0.8}Sr_{0.2}MnO_3$ also has been confirmed with the TGA test (shown in Figure S1).[35, 36] For comparison, we also prepared the catalyst ink by mixing 5 mg 5wt% $IrO_2$-$La_{0.8}Sr_{0.2}MnO_3$ (LSMI5) catalyst with 5 mg carbon black,[33] which was also dispersed

in 1 mL 0.05 wt% Nafion®117 aqueous solution and sonicated for several minutes to form uniform slurry. The working electrode was prepared by loading 10 μL catalyst ink onto the glassy carbon (5 mm diameter) rotating disk electrode (RDE), which was dried in air for 30 mins. Linear sweep scan curves for OER were performed at 1600 rpm in 0.1 mol $L^{-1}$ KOH solution from 0-1 V vs Ag/AgCl at a scan speed of 10 mV $s^{-1}$. The ORR test was carried out in $O_2$-saturated electrolyte at different rotation speeds from -0.8-0.2 V with the same scan rate as OER. The electrochemical impedance spectra (EIS) were tested at 0.8 V vs Ag(s)|AgCl(s) (3.5 mol $L^{-1}$ KCl) with frequencies ranging from 100 kHz to 0.1 Hz with an amplitude of 5 mV. The obtained potential values vs Ag/AgCl were converted to the reversible hydrogen electrode (RHE) based on the Nernst Equation (1) and corrected by iR compensation according to equation (2)

$$E_{RHE} = 0.197 + E_{Ag/AgCl} + 0.059 \times pH_{electrolyte} \quad (1)$$

$$E_{iRcorrected} = E - iR \quad (2)$$

where 'i' is the measured current density and 'R' the ohmic resistance of electrolyte solution, which was measured by AC Impedance in 0.1 mol $L^{-1}$ KOH aqueous solution.

The ORR mechanism can be further examined using the Koutecky−Levich (K-L) equation, which is labeled as equation (3).

$$\frac{1}{J} = \frac{1}{J_k} + \frac{1}{J_L} = \frac{1}{nFkC^0} + \frac{1}{0.62nFD_{O_2}{}^{2/3}\nu^{-1/6}C^0\omega^{1/2}} \quad (3)$$

Where $J$, $J_k$ and $J_L$ are the disk current density, the kinetic and the film diffusion-limiting current density, respectively. Besides, $n$ is the number of electrons transferred in the ORR process, $F$ is the Faraday constant (96500 C $mol^{-1}$), $C^0$ is the saturated concentration of oxygen in 0.1 mol $L^{-1}$ KOH, $\omega$ is the rotating rate (rad $s^{-1}$), $D_{O2}$ is the oxygen diffusion coefficient ($1.73\times10^{-5}$ $cm^2$ $s^{-1}$)[33],

$v$ is the kinetic viscosity of the electrolyte solution ($0.01 cm^2 s^{-1}$) and $k$ is the rate constant for ORR. The number of electron transfer can be calculated based on this K-L plot.

**3. Results and discussion**

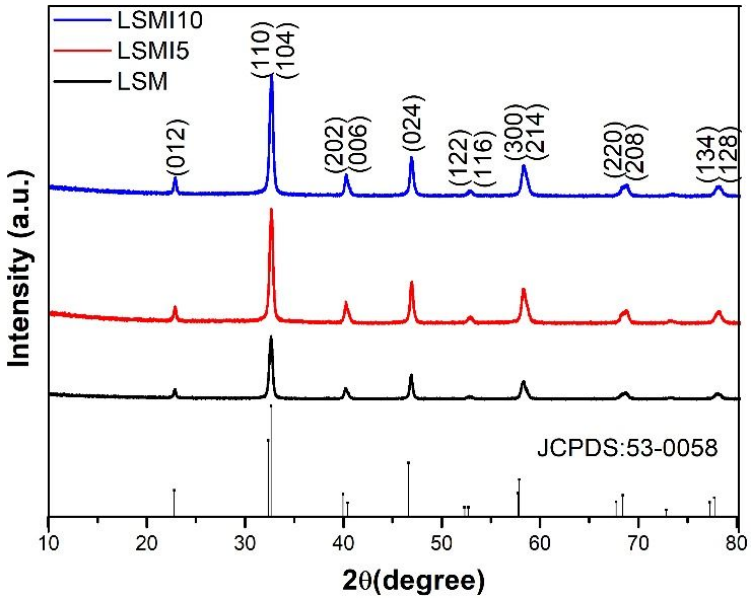


Figure 1. The XRD patterns of the pristine $La_{0.8}Sr_{0.2}MnO_3$ (LSM), 5 wt% $IrO_2$-incorporated $La_{0.8}Sr_{0.2}MnO_3$, (LSMI5) and 10 wt% $IrO_2$-$La_{0.8}Sr_{0.2}MnO_3$, (LSMI10).

X-ray diffraction (XRD) was used to examine the composition and crystal structure of the as-prepared materials, including the pristine $La_{0.8}Sr_{0.2}MnO_3$ and both 5 wt% and 10 wt% $IrO_2$-incorporated $La_{0.8}Sr_{0.2}MnO_3$, as shown in Figure 1, in which the vertical lines are the peak positions from the standard JSPDS card (No. 53-0058). Compared with the standard card, all the diffraction peaks of the pristine $La_{0.8}Sr_{0.2}MnO_3$ could be indexed to a rhombohedral phase. No extra peaks corresponding to metallic phases were detected from the pristine $La_{0.8}Sr_{0.2}MnO_3$, which means that the samples are pure rhombohedral phase perovskites. It was also observed that even with the incorporation $IrO_2$, no obvious diffraction peaks from $IrO_2$ appeared in both $IrO_2$-incorporated $La_{0.8}Sr_{0.2}MnO_3$ samples, which might be ascribed to the very small amount of $IrO_2$ in the composites, which is similar to the previous report,[27] since for 5 wt% $IrO_2$-$La_{0.8}Sr_{0.2}MnO_3$

material, Iridium element accounts for a very small amount (0.40 mol%) of the entire sample as determined semi-quantitatively by the Energy dispersive x-ray spectroscopy (EDS) analysis. Furthermore, the XRD peaks of $IrO_2$-incorporated $La_{0.8}Sr_{0.2}MnO_3$ at the position of 2Θ around 47° show slight shift to higher diffraction angles (Figure S2), which excludes the possibility that Ir goes into the Mn site in $La_{0.8}Sr_{0.2}MnO_3$ since the radius of $Ir^{4+}$ (76 pm) is larger than that of $Mn^{3+}$ (72 pm),[31] which will cause the lattice expansion, resulting in XRD peaks shift to lower angles.

Figure 2a shows the TEM image of the 5 wt% $IrO_2$-$La_{0.8}Sr_{0.2}MnO_3$, from which we can see its particle size ranges from 20-80 nm. However, we cannot distinguish the $IrO_2$ nanoparticles from $La_{0.8}Sr_{0.2}MnO_3$ in the low magnification TEM, which might be due to the similar contrast of the particles under electron beam radiation. While in the HRTEM images, there are two different lattice diffraction fringes inside the composite, which are measured to be 0.277 nm and 0.315 nm, corresponding to the d-spacing of (110) plane of $La_{0.8}Sr_{0.2}MnO_3$[4] and (110) plane of $IrO_2$,[30] respectively, which indicates the existence of $IrO_2$ inside the composite. EDS was also carried out to analyze the chemical elemental composition in the as-prepared electrocatalysts. As shown in Figure 2c-h, it is confirmed by the EDS mapping and the corresponding spectroscopy that Iridium (Ir), Lanthanum (La), Strontium (Sr) and Manganese (Mn) distribute homogeneously in 5 wt% $IrO_2$-$La_{0.8}Sr_{0.2}MnO_3$, while for the pristine $La_{0.8}Sr_{0.2}MnO_3$, no Iridium was observed and only La, Sr and Mn were detected on the surface of the sample (Figure S3). Besides, there is only one lattice fringe (d=0.276 nm) in the HRTEM image (Figure S3b), which agrees well with the (110) interplanar spacing of the $La_{0.8}Sr_{0.2}MnO_3$.[37] In addition, surface area is also an important parameter to characterize the catalysts. It is generally accepted that catalysts with high surface area will expose more active sites to the reactants, leading to higher reaction rate and thus better electrocatalytic performance. Thus, BET test was employed to measure the surface areas of the as-

prepared perovskite oxides composite. As shown in Figure S4, the specific surface area of the pristine $La_{0.8}Sr_{0.2}MnO_3$ is 19.2 $m^2/g$ while the surface areas of 5 wt% $IrO_2$-$La_{0.8}Sr_{0.2}MnO_3$ and 10 wt% $IrO_2$-$La_{0.8}Sr_{0.2}MnO_3$ are 23.3 and 20.7 $m^2/g$, respectively. The trend of the surface areas with the $IrO_2$ incorporation is consistent with previous reports.[30, 38] This increased surface area of the $IrO_2$ incorporated $La_{0.8}Sr_{0.2}MnO_3$ indicates that more active sites can be exposed to contact with the reactants and thus faster reaction rate and better electrocatalytic performance compared to the pristine $La_{0.8}Sr_{0.2}MnO_3$.

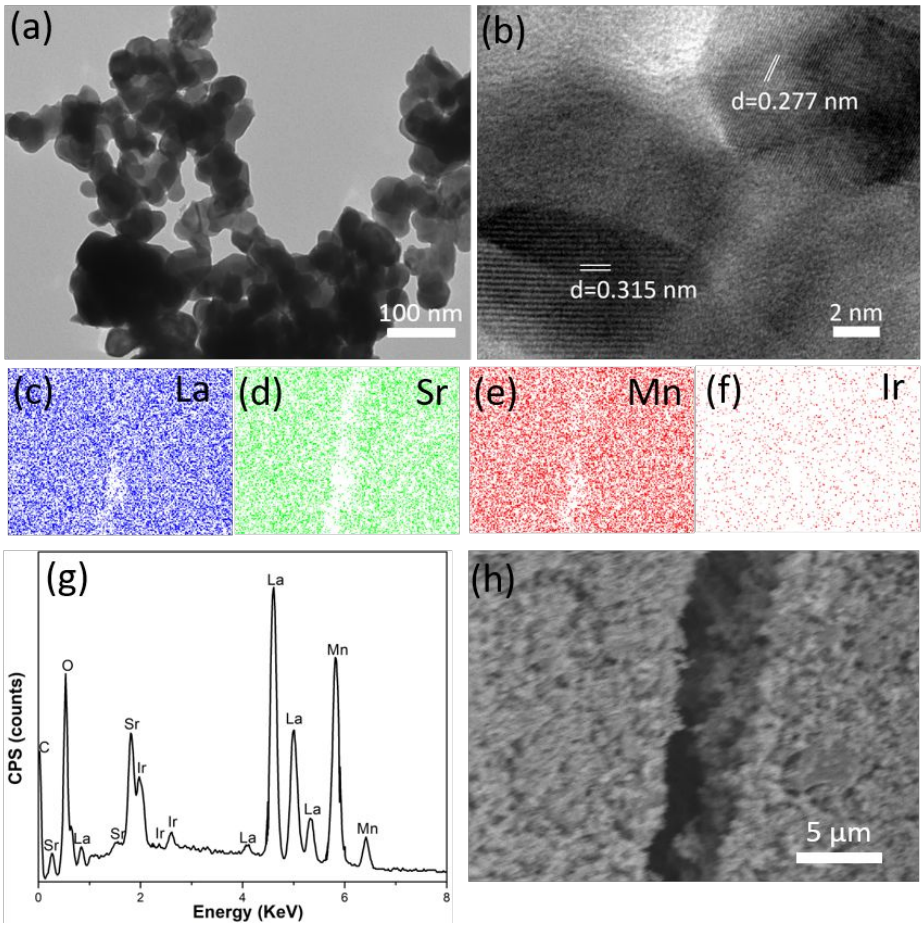


Figure 2. TEM (a) and HRTEM (b) images of 5 wt% $IrO_2$-$La_{0.8}Sr_{0.2}MnO_3$; SEM image (h) with the corresponding EDS mapping of (c) La, (d) Sr, (e) Mn, (f) Ir and (g) EDS spectrum of the same 5 wt% $IrO_2$-$La_{0.8}Sr_{0.2}MnO_3$.

X-ray photoelectron spectroscopy (XPS) can also be used to investigate the elemental composition on the surface of the samples. The presence of $IrO_2$ in the 5 wt% $IrO_2$-$La_{0.8}Sr_{0.2}MnO_3$ composite could be further confirmed using XPS. The entire XPS survey scan is shown in Figure S5, if we compare the scan spectroscopy of the 5 wt% $IrO_2$-$La_{0.8}Sr_{0.2}MnO_3$ to the pristine $La_{0.8}Sr_{0.2}MnO_3$, several extra peaks appeared in the 5 wt% $IrO_2$-$La_{0.8}Sr_{0.2}MnO_3$, which can be assigned to different Iridium peaks.[30] Especially the characteristic peak Ir 4f located at around 60-70 eV, is absent in the pristine $La_{0.8}Sr_{0.2}MnO_3$ (Figure 3a). The peak located at around 61.81 eV corresponds to the binding energy of Ir $4f_{7/2}$ in $IrO_2$ while the peak with a binding energy of 64.71 eV can be attributed to Iridium $4f_{5/2}$ of $IrO_2$, which are consistent with the previous reports.[39] When we enlarge the region from 40-80 eV, indicated in Figure 3b, Ir $4f_{7/2}$ could be further deconvoluted into two peaks located at 62.3 and 61.81 eV, which can be assigned to $Ir^{3+}$ and $Ir^{4+}$ ($IrO_2$), respectively,[30, 40] consistent with the previous report that even commercial $IrO_2$ contains certain amount of $Ir^{3+}$ at the outlayer.[40] Based on the above characterization and analysis results, it can be concluded that $IrO_2$ has been successfully incorporated into $La_{0.8}Sr_{0.2}MnO_3$ sample.

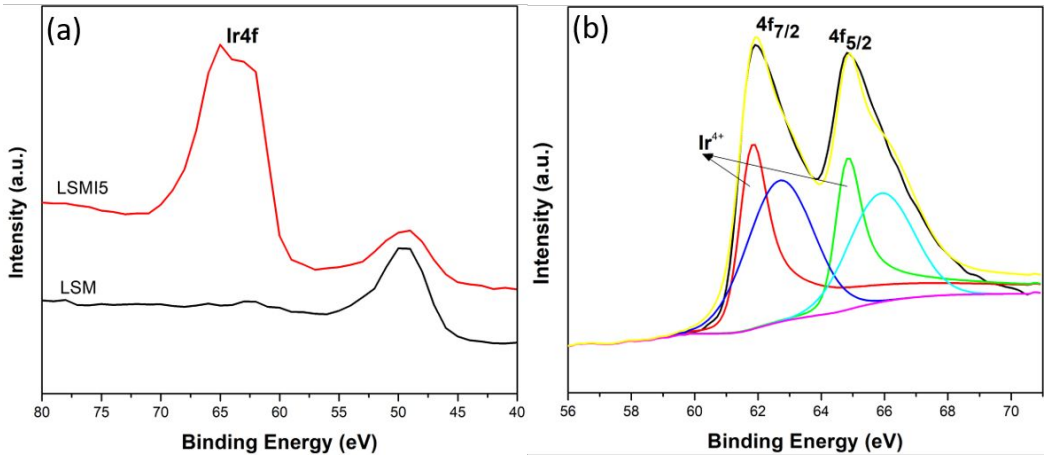


Figure 3. (a) XPS spectra comparison (40-80 eV region) for the pristine $La_{0.8}Sr_{0.2}MnO_3$ and 5 wt% $IrO_2$-$La_{0.8}Sr_{0.2}MnO_3$ from the survey scan and (b) representative fitting for Ir4f spectra in $IrO_2$ for 5 wt% $IrO_2$-$La_{0.8}Sr_{0.2}MnO_3$.

The electrocatalytic behavior of the as-prepared three materials for oxygen reduction reaction (ORR) have been examined in $O_2$-saturated 0.1 mol $L^{-1}$ KOH solution using linear sweep voltammetry (LSV) technique with RDE. Figure S6 shows the LSV polarization curves of the pristine $La_{0.8}Sr_{0.2}MnO_3$, 5 wt% $IrO_2$-$La_{0.8}Sr_{0.2}MnO_3$ and 10 wt% $IrO_2$-$La_{0.8}Sr_{0.2}MnO_3$ in $O_2$-saturated 0.1 mol $L^{-1}$ KOH with a scan rate of 10 mV $s^{-1}$ under four different rotation rates (100, 400, 900 and 1600 rpm). The current density increases gradually with the increased rotation rates. The current densities comparison of ORR for the as-prepared materials at a rotation rate of 1600 rpm are displayed in Figure 4a. It is clear that the $IrO_2$-incorporated $La_{0.8}Sr_{0.2}MnO_3$ shows larger current density than the pure $La_{0.8}Sr_{0.2}MnO_3$. The higher current density shows the superior ORR electrocatalytic performance of the $IrO_2$-incorporated $La_{0.8}Sr_{0.2}MnO_3$. The diffusion limiting current densities of the pristine $La_{0.8}Sr_{0.2}MnO_3$ and (5 wt% and 10 wt%) $IrO_2$-$La_{0.8}Sr_{0.2}MnO_3$ are 4.2, 5.2 and 5.8 mA $cm^{-2}$, respectively, which can further confirm the better ORR electrocatalytic performance of the $IrO_2$-$La_{0.8}Sr_{0.2}MnO_3$. To compare the performance of the as-prepared perovskites with/without extra conductive carbon, the ORR performance of the pure LMSI5 and LSMI5+carbon black also has been conducted and performance comparison between them is displayed in Figure S7(a). It can be seen that when we introduced extra carbon black into the electrocatalyst, there is only very slight increase in current densities of the LSV for ORR, which might be due to the increased conductivity of the materials due to the addition of extra carbon. This slight increase in the current density also indicates that the conductivity of our sample prepared using polymer-assisted method is good enough to be used as electrocatalyst directly without adding extra carbon in order to avoid the complicated procedures. This is further confirmed from the OER performance comparison among the LSMI5 and LSMI5+carbon black,

shown in Figure S7 (b), which also showed slight current density increase in OER of LSMI5+carbon black compared with the pristine LSMI5.

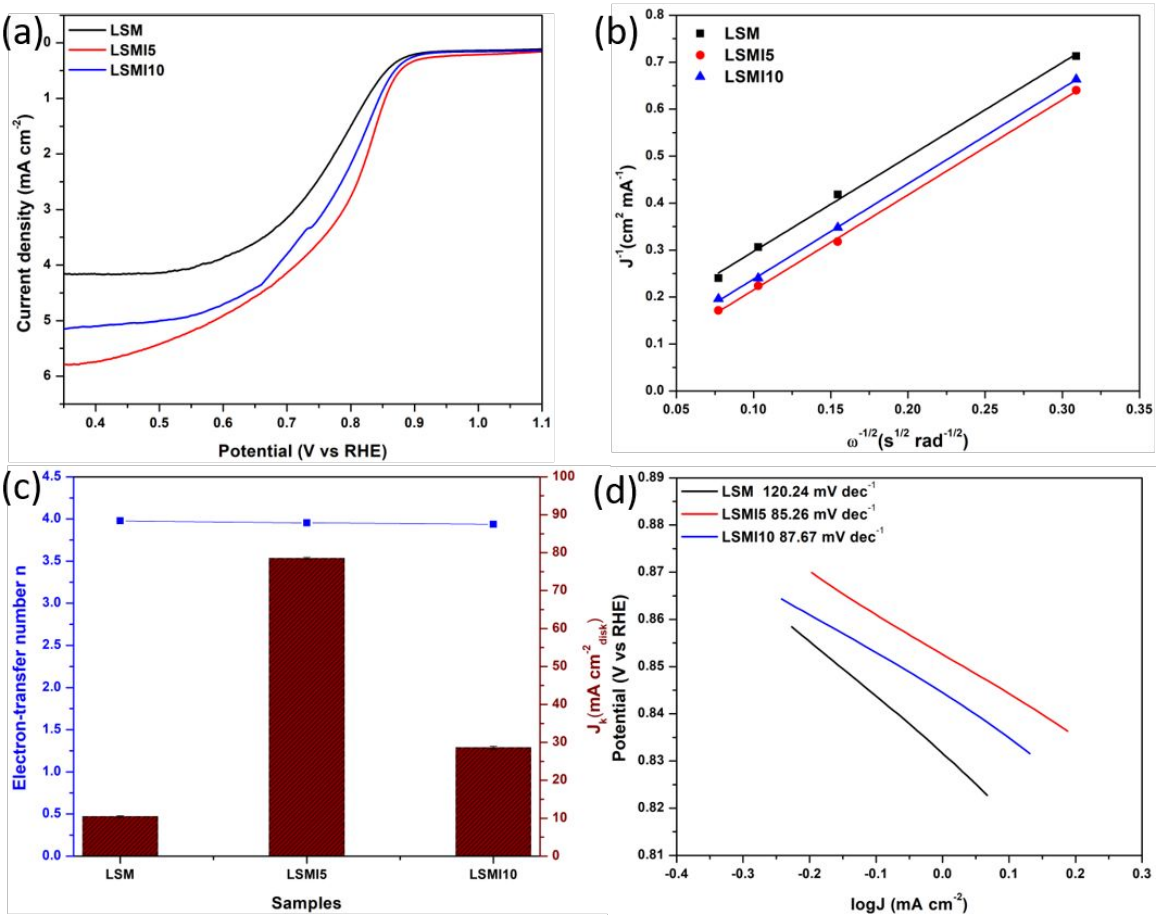


Figure 4. (a) ORR polarization curves of three samples: $La_{0.8}Sr_{0.2}MnO_3$ (LSM), 5 wt% $IrO_2$-$La_{0.8}Sr_{0.2}MnO_3$ (LSMI5) and 10 wt%-$La_{0.8}Sr_{0.2}MnO_3$ (LSMI10) with a rotating speed of 1600 rpm; (b) Koutecky-Levich plots of three samples at 0.4 V vs RHE derived from the ORR results at Figure S3; (c) the electron transfer number and the kinetic current density of the samples at 0.4 V vs RHE; and (d) Tafel plots for the as-prepared samples.

In order to study the electrocatalytic behavior and kinetic process in the ORR of the as-prepared catalysts, Koutecky-Levich (K-L) plots have been derived from the LSV polarization curves (Figure S3), which show a first-order relationship between $J^{-1}$ and $\omega^{-1/2}$. The number (n) of electron transfer in ORR at 0.4 V (vs RHE) calculated using the slope of the K-L plots (Figure 4b) is approximately 3.98, 3.95 and 3.93 for the pristine $La_{0.2}Sr_{0.8}MnO_3$ and 5 wt%, 10 wt% $IrO_2$-

incorported $La_{0.8}Sr_{0.2}MnO_3$, respectively, which are indicated in Figure 4c. It is generally accepted that when the ORR follows a four-electron transfer reaction ($O_2 + H_2O + 4e^- = 4OH^-$), the n value is expected to be four. Therefore, the estimated n values of the as-prepared materials, which are all close to four, indicate that four-electron transfer pathway dominates in the ORR reactions of the catalysts rather than formation of the intermediate species of $HO_2^-$.[33] Besides, the kinetic current density (Figure 4c) of the catalysts can also be extrapolated from the K-L plots. Combined with Tafel plots in Figure 4d, more information regarding the ORR reaction rate of the catalysts can be obtained. The increased $J_k$ and the decreased Tafel slope in the sequence of 5 wt% $IrO_2$-$La_{0.8}Sr_{0.2}MnO_3$, 10 wt % $IrO_2$-$La_{0.8}Sr_{0.2}MnO_3$ and $La_{0.8}Sr_{0.2}MnO_3$ can indicate faster ORR reaction rate, which further reflects the enhanced ORR performance with $IrO_2$ incorporation.

Based on the above analysis, conclusion that can be reached is $IrO_2$-incorporated $La_{0.8}Sr_{0.2}MnO_3$ composites showed superior ORR electrocatalytic performance compared with the pristine $La_{0.8}Sr_{0.2}MnO_3$. Besides, 5 wt% $IrO_2$-$La_{0.8}Sr_{0.2}MnO_3$ showed slightly better ORR catalytic performance than 10 wt% $IrO_2$-$La_{0.8}Sr_{0.2}MnO_3$. The enhanced electrocatalytic performance of $IrO_2$-incorporated $La_{0.8}Sr_{0.2}MnO_3$ might be due to the synergistic effect between the good OER performance of $IrO_2$ and high ORR catalytic activity of $La_{0.8}Sr_{0.2}MnO_3$. However, too much (10 wt%) $IrO_2$-$La_{0.8}Sr_{0.2}MnO_3$ might result in less synergistic effect as well as reduced conductivity of the mixed metal oxide composites, which leads to the reduced electrocatalytic performance compared with 5 wt% $IrO_2$-$La_{0.8}Sr_{0.2}MnO_3$, as reported in literatures for $IrO_2$-$TiO_2$ and $IrO_2$-$MoO_3$ composites.[29, 30, 38]

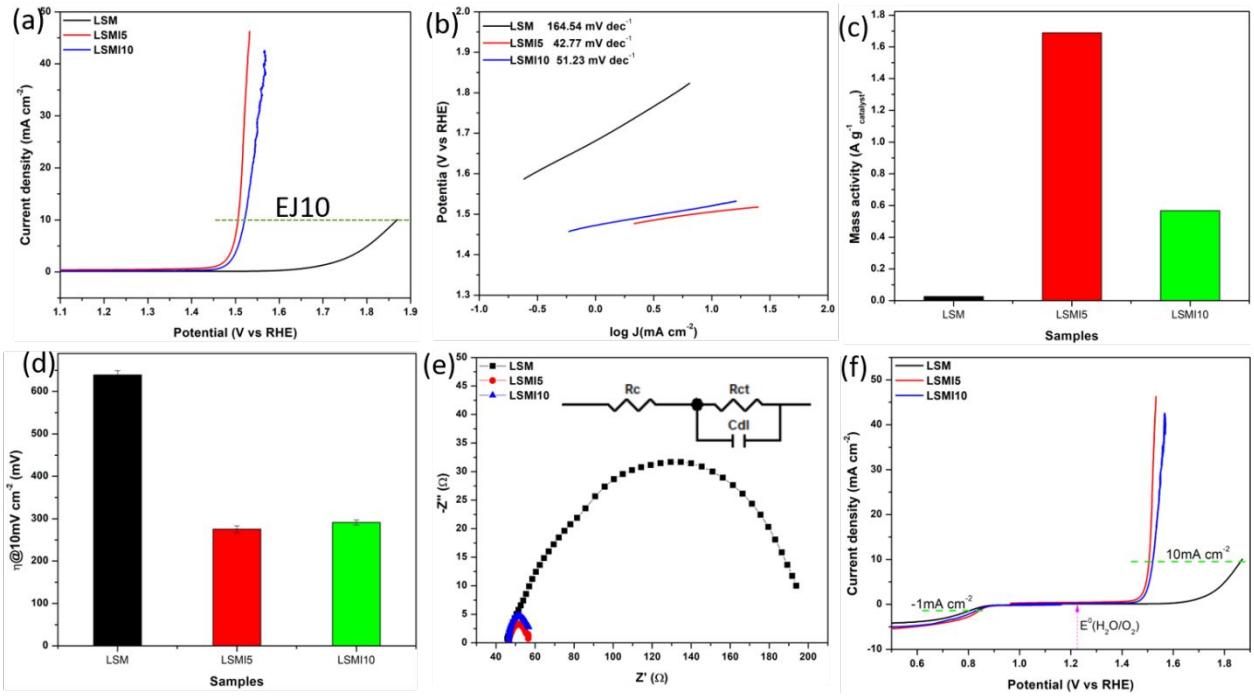


Figure 5. (a) OER polarization curves for three samples: the pristine $La_{0.8}Sr_{0.2}MnO_3$ and the $IrO_2$ (5 wt% and 10 wt%) incorporated $La_{0.8}Sr_{0.2}MnO_3$ in 0.1 mol $L^{-1}$ KOH solution; (b) Tafel plots of the three samples; (c) Mass activity of the three samples at 1.53 V vs RHE; (d) Overpotential @ 10 mA $cm^{-2}$ comparison of the pristine and two (5 wt% and 10 wt%) $IrO_2$-incorporated $La_{0.8}Sr_{0.2}MnO_3$; (e) Nyquist plots of the three samples at 1.76 V vs RHE with an amplitude of 5 mV with the equivalent electrical circuit inserted; and (f) Bifunctional catalytic activity comparison for both OER and ORR of the three samples: the pristine $La_{0.8}Sr_{0.2}MnO_3$ and the $IrO_2$ (5 wt% and 10 wt%)-incorporated $La_{0.8}Sr_{0.2}MnO_3$.

To evaluate the bifunctionality of the as-prepared materials as oxygen electrocatalysts for both OER and ORR, OER polarization curves were tested in 0.1 mol $L^{-1}$ KOH solution at a scan rate of 10 mV $s^{-1}$. The onset potential (potential at which the evolution is started or the current density starts increasing)[41] is an important parameter to compare the OER performance of the electrocatalysts. As shown in Figure 5a, 5 wt% $IrO_2$- $La_{0.8}Sr_{0.2}MnO_3$ exhibits lower onset potential (1.44 V vs RHE) and larger catalytic current density than that of the 10 wt% $IrO_2$-$La_{0.8}Sr_{0.2}MnO_3$ (1.45 V vs RHE) and the pristine $La_{0.8}Sr_{0.2}MnO_3$ (1.60 V vs RHE), indicating better OER performance with the $IrO_2$ incorporation. It is also noted that 5 wt% $IrO_2$-$La_{0.8}Sr_{0.2}MnO_3$ has better

performance than the pristine pure $La_{0.8}Sr_{0.2}MnO_3$ while when the $IrO_2/La_{0.8}Sr_{0.2}MnO_3$ weight ratio has increased to 10 wt%, the OER current density decreased a little compared with 5 wt% $IrO_2$-$La_{0.8}Sr_{0.2}MnO_3$, even though still showed superior performance than the pristine pure $La_{0.8}Sr_{0.2}MnO_3$. This phenomenon may be attributed to the synergistic effect between the two materials while too much $IrO_2$ existing in the mixture of $IrO_2/La_{0.8}Sr_{0.2}MnO_3$ might lead to less synergistic effect and conductivity[29, 30] of the metal oxides composites. It might also be due to the decreased surface area of the 10 wt% incorporated $La_{0.8}Sr_{0.2}MnO_3$ compared with 5 wt% $IrO_2$-$La_{0.8}Sr_{0.2}MnO_3$, which is consistent with previously reported work.[30, 38] In addition, the enhanced electron transfer due to the establishment of good conductive network among the interface between $IrO_2$ and $La_{0.8}Sr_{0.2}MnO_3$ is also believed to be responsible for the better OER catalytic performance of 5 wt% $IrO_2$-$La_{0.8}Sr_{0.2}MnO_3$.[30, 42]

Furthermore, EJ10 (the potential to achieve the current density of 10 mA $cm^{-2}$) has also been compared among the catalysts (Figure 5a). 5 wt% $IrO_2$-$La_{0.8}Sr_{0.2}MnO_3$ can achieve this current density at about 1.506 V (vs RHE), lower than both the 10 wt% $IrO_2$-$La_{0.8}Sr_{0.2}MnO_3$ (1.521 V vs RHE) and the $La_{0.8}Sr_{0.2}MnO_3$ (1.86 V vs RHE), which suggests that 5 wt% $IrO_2$-$La_{0.8}Sr_{0.2}MnO_3$ shows the best OER electrocatalytic performance among the three materials. Besides, EJ10 of 5 wt% $IrO_2$-$La_{0.8}Sr_{0.2}MnO_3$ is even lower than the pure $IrO_2$ (Table 1), as reported before.[30] In addition to the synergistic effect among $IrO_2$ and $La_{0.8}Sr_{0.2}MnO_3$, the improved electrocatalytic activity of LSMI5 compared to the pure $IrO_2$ might be also due to the stabilization of small $IrO_2$ particles on $La_{0.8}Sr_{0.2}MnO_3$ and the associated particle-support interactions between $IrO_2$ and $La_{0.8}Sr_{0.2}MnO_3$,[29] the increased specific surface area (Figure S6) and ECSA (Figure 6) as well as the interfacial effect among $IrO_2$ and $La_{0.8}Sr_{0.2}MnO_3$, which can facilitate the electron transportation,[30] leading to better electrocatalytic performance. Furthermore, the Tafel slope

(Figure 5b) of 5 wt% $IrO_2$-$La_{0.8}Sr_{0.2}MnO_3$ is much smaller (42.8 mV $dec^{-1}$) than both the 10 wt% $IrO_2$-$La_{0.8}Sr_{0.2}MnO_3$ (51.2 mV $dec^{-1}$) and the pristine $La_{0.8}Sr_{0.2}MnO_3$ (164.5 mV $dec^{-1}$), also indicating faster OER rate. The mass activity (Figure 5c) of each catalyst at 1.53 V vs RHE can be obtained by normalizing the OER current with the catalyst loading, the trend of which is consistent with the OER activities.

The overpotential η at a current density of 10 mA $cm^{-2}$ (Figure 5d) is a widely used indicator to evaluate the electrocatalytic performance of perovskite oxides.[43] Obviously, a lower overpotential is obtained for the 5 wt% and 10 wt% $IrO_2$-$La_{0.8}Sr_{0.2}MnO_3$ (275 and 291 mV) than that for the pristine $La_{0.8}Sr_{0.2}MnO_3$ (639 mV). 5 wt% $IrO_2$-$La_{0.8}Sr_{0.2}MnO_3$ exhibits much smaller overpotential than the reported perovskite oxide electrocatalysts[19] and showed the best OER activity among the three samples, consistent with the previous analysis above. Finally, the electrochemical impedance spectroscopy (EIS) (Figure 5e) of the as-prepared catalysts were also performed and the equivalent circuit of the EIS is inserted. Rct is the charge transfer resistance, Rs stands for the solution resistance and Cdl is the constant phase element. $IrO_2$-incorporated $La_{0.8}Sr_{0.2}MnO_3$ composites have smaller semicircle radius and charge transfer resistance Rct (8.64 Ω for 5 wt% $IrO_2$-$La_{0.8}Sr_{0.2}MnO_3$) than the pristine $La_{0.8}Sr_{0.2}MnO_3$ (101.6 Ω), which suggests higher charge-transfer ability and thus faster catalytic rate, consistent with the OER results (Figure 5a).

The total overpotential ($\Delta E = E_{J10}-E_{J-1}$) between $E_{J10}$ (the potential at 10 mA $cm^{-2}$ for OER) and $E_{J-1}$ (potential at -1 mA $cm^{-2}$ for ORR) can be regarded as the indicator to evaluate the bifunctionality of the catalysts. It is generally accepted that smaller ΔE indicates higher bifunctional electrocatalytic activity. The bifunctional performance of 5 wt% $IrO_2$-$La_{0.8}Sr_{0.2}MnO_3$ is superior to that of both 10 wt% $IrO_2$-$La_{0.8}Sr_{0.2}MnO_3$ and $La_{0.8}Sr_{0.2}MnO_3$ based on the ΔE values

obtained from Figure 5f, which are 0.652, 0.677 and 1.043 V, respectively. The ΔE value of $IrO_2$-incorporated $La_{0.8}Sr_{0.2}MnO_3$ indicates that the incorporation of $IrO_2$ can indeed enhance the bifunctionality of the catalysts due to the synergistic effect between the two materials. Besides, the ΔE value is much smaller than the reported state-of-the-art electrocatalysts (Table 1), including both perovskites, Pt/C and $IrO_2$, which indicates that superior bifunctional performance of the $IrO_2$-incorporated $La_{0.8}Sr_{0.2}MnO_3$.

Table 1. The bifunctional electrocatalytic activity comparison between the pristine and $IrO_2$-incorporated $La_{0.8}Sr_{0.2}MnO_3$ catalysts and the reported noble-metal/perovskite-based catalysts. All the tests for the catalysts were conducted in 0.1 mol $L^{-1}$ KOH solution.

| Electrocatalysts | Scan rate | $E_{ORR}$@-1mA $cm^{-2}$/V | $E_{OER}$@10mA $cm^{-2}$/V | ΔE (V, $E_{ORR}$-$E_{OER}$) | Reference |
|---|---|---|---|---|---|
| $La_{0.8}Sr_{0.2}MnO_3$ | 10 mV $s^{-1}$ | 0.825 vs RHE | 1.869 vs RHE | 1.043 | This work |
| $La_{0.8}Sr_{0.2}MnO_3$-5 wt% $IrO_2$ | 10 mV $s^{-1}$ | 0.854 vs RHE | 1.506 vs RHE | 0.652 | This work |
| $La_{0.8}Sr_{0.2}MnO_3$-10 wt% $IrO_2$ | 10 mV $s^{-1}$ | 0.844 vs RHE | 1.521 vs RHE | 0.677 | This work |
| $LaCo_{0.5}Ni_{0.5}O_3$ | 10 mV $s^{-1}$ | -0.22 vs Ag/AgCl | 0.66 vs Ag/AgCl | 0.88 | 11 |
| $La_{0.95}FeO_3$ | 10 mV $s^{-1}$ | 0.58 vs RHE | 1.64 vs RHE | 1.06 | 20 |
| $La_{0.6}Sr_{0.4}CoO_{3-\delta}$ | 5 mV $s^{-1}$ | -0.196 vs Hg/HgO | 0.921vs Hg/HgO | 1.12 | 44 |
| $La_{0.8}Sr_{0.2}MnO_3$ | 10 mV $s^{-1}$ | -0.13 vs Ag/AgCl | 0.95 vs Ag/AgCl | 1.08 | 31 |
| $(La_{0.8}Sr_{0.2})_{0.95}Mn_{0.95}Ir_{0.05}O_3$ | 10 mV $s^{-1}$ | -0.1 vs Ag/AgCl | 0.71 vs Ag/AgCl | 0.81 | 31 |
| $BaTiO_3$ | 5 mV $s^{-1}$ | 0.72 vs RHE | 1.90 vs RHE | 1.18 | 45 |
| $LaNiO_3$-$Fe_2O_3$ | 10 mV $s^{-1}$ | 0.71 vs RHE | 1.65 vs RHE | 0.94 | 27 |
| Pt/C | 10 mV $s^{-1}$ | 0.97 vs RHE | 2.19 vs RHE | 1.22 | 46 |
| $IrO_2$ | 10 mV $s^{-1}$ | 0.38 vs RHE | 1.70 vs RHE | 1.32 | 46 |

Besides the synergistic effect among $IrO_2$ and $La_{0.8}Sr_{0.2}MnO_3$, it is believed that the electrochemically active surface area (ECSA) of the as-synthesized electrocatalysts are also responsible for the improved performance of the $IrO_2$-incorporated $La_{0.8}Sr_{0.2}MnO_3$. Therefore, the ECSA of electrocatalysts can be assessed using the double layer capacitance, which is widely adopted.[11, 19] The double layer capacitance could be obtained by measuring cyclic voltammetry (CV) at different scan rates in the non-faradaic region, which are demonstrated in Figure 6. By

plotting the capacitive current densities as a function of the scan rates, nearly linear curves (Figure 6d) could be obtained, the slope of which represents the double layer capacitance, which could further indicate the ECSA since it is challenging to obtain the accurate ECSA values for materials with multi-composites.[46] The capacitance of 5 wt% $IrO_2$-$La_{0.8}Sr_{0.2}MnO_3$ obtained from Figure 6d is 10.562 mF $cm^{-2}$, larger than that of 10 wt% $IrO_2$-$La_{0.8}Sr_{0.2}MnO_3$ (6.4136mF $cm^{-2}$) as well as the pristine $La_{0.8}Sr_{0.2}MnO_3$ (2.1135 mF $cm^{-2}$). Therefore, 5 wt% $IrO_2$-$La_{0.8}Sr_{0.2}MnO_3$ exhibits the largest ECSA and thus best OER catalytic activity towards water splitting among the three materials since a high number of active sites would be exposed to electrolyte for electrocatalysis, which is in good agreement with the electrocatalytic experimental results discussed above.

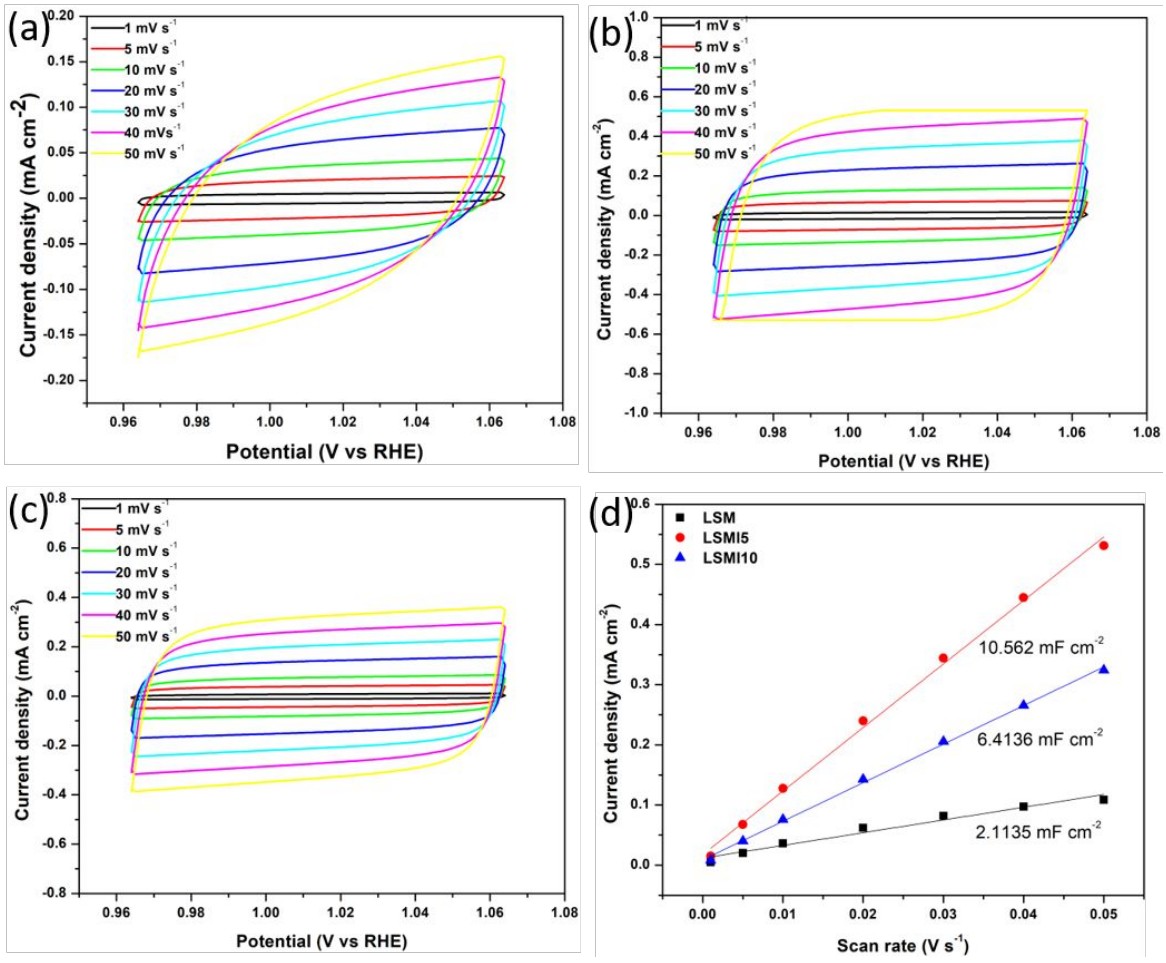

Figure 6. Double-layer capacitance measurements for determining electrochemically active surface area for the as-prepared catalysts: (a) $La_{0.8}Sr_{0.2}MnO_3$, (b) 5 wt% $IrO_2$-$La_{0.8}Sr_{0.2}MnO_3$, (c) 10 wt% $IrO_2$-$La_{0.8}Sr_{0.2}MnO_3$ using cyclic voltammetry in 0.1 mol $L^{-1}$ KOH aqueous solution in a non-Faradaic region at different scan rates as indicated; and (d) The cathodic charging currents measured at 1.45 V vs RHE as a function of scan rates.

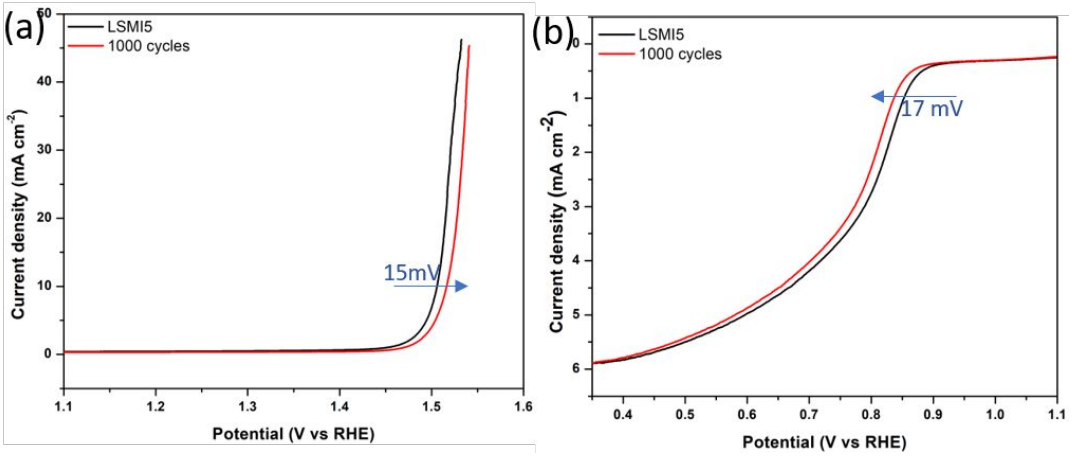


Figure 7. Stability test of 5 wt% $IrO_2$-$La_{0.8}Sr_{0.2}MnO_3$. LSVs of OER (a) and ORR (b) tested in $O_2$-saturated 0.1 mol $L^{-1}$ KOH solution before and after 1000 cycles at a sweep rate of 10 mV $s^{-1}$ with a rotation speed of 1600 rpm.

Stability is an important parameter to evaluate the practical applicability of the electrocatalysts. To examine the stability of the 5 wt% $IrO_2$-$La_{0.8}Sr_{0.2}MnO_3$, continuous cycling voltammetry scans between 0.1-1.9 V (vs. RHE) in 0.1 mol $L^{-1}$ KOH at a scan rate of 10 mV $s^{-1}$ have been conducted for 1000 cycles and the LSVs of the electrocatalysts have been measured before and after the cycles. Compared with the initial LSV scan, the potential (Figure 7) to achieve 10 mA $cm^{-2}$ for OER after 1000 cycles shifted about 15 mV to the higher voltage and 17 mV negative shift appeared to reach -1 mA $cm^{-2}$ for ORR. This indicates the good durability of 5 wt% $IrO_2$-$La_{0.8}Sr_{0.2}MnO_3$ in alkaline solution. The stability test (Figure S8) for $La_{0.8}Sr_{0.2}MnO_3$ and 10 wt% $IrO_2$-$La_{0.8}Sr_{0.2}MnO_3$ were also conducted and showed comparatively high stability, which implies that the as-prepared materials have the potential to be candidates as oxygen catalysts in fuel cell or metal-air batteries.

## 4. Conclusion

In summary, a novel composite electrocatalyst $IrO_2$-incorporated $La_{0.8}Sr_{0.2}MnO_3$ has been proposed and synthesized for the first time to the best of our knowledge to be bifunctional oxygen electrocatalyst. Compared with the pristine $La_{0.8}Sr_{0.2}MnO_3$, the bifunctional oxygen electrocatalytic performance could be enhanced with the incorporation of $IrO_2$, which might be due to the synergistic effect between the good OER performance of pure $IrO_2$ and the ORR electrocatalytic activity of $La_{0.8}Sr_{0.2}MnO_3$ as well as the increased ECSA of the electrocatalysts. The bifunctionality of the composites is comparable or even better than the current state-of-the-art electrocatalysts reported recently. Besides, the new electrocatalysts also showed comparatively high stability under alkaline medium (15 mV positive shift for achieving 10 mA $cm^{-2}$ for OER and 17 mV negative shift to reach -1 mA $cm^{-2}$ in ORR for 5 wt% incorporated $La_{0.8}Sr_{0.2}MnO_3$), which indicates their potential applications in both fuel cells and metal-oxygen batteries. Our study not only introduces a new composite material as bifunctional oxygen electrocatalyst for both OER and ORR but also opens a new way to enhance the electrocatalytic activity of perovskite metal oxides.

## Supporting information

Electronic Supplementary Information (ESI) available: [Additional information regarding the Figure S1-S8 are presented in the Supporting Information section].

## Conflicts of interest

There are no conflicts to declare.

## Acknowledgements

Dr. Luo thanks the support from USDA National Institute of Food and Agriculture, HSI Collaboration: Integrating Food Science/Engineering and Education Network (IFSEEN, award

number: 2015-38422-24059). This work is also supported by the Idaho National Laboratory Directed Research and Development Program under DOE Idaho Operations Office Contract DE-AC07-05ID14517.

## References

[1]. X.J. Zheng, J. Wu, X.C. Cao, J. Abbott, C. Jin, H.B. Wang, P. Strasser, R.Z. Yang, X. Chen, G. Wu, *Appl. Catal. B-Environ*, 2018, **241,** 442-451.
[2]. M.J. Chen, L. Wang, H.P. Yang, S. Zhao, H. Xu, G. Wu, *J. Power Sources*, 2017, **375,** 277-290.
[3]. S. Gupta, W. Kellogg, H. Xu, X. Liu, J. Cho, G. Wu, *Chem. Asian. J.* , 2016, **11,** 10-21.
[4]. W.C. Xu, L.T. Yan, L. Teich, S. Liaw, M. Zhou, H.M. Luo, *Electrochim. Acta*, 2018, **273,** 80-87.
[5]. C.C. Xu, P. Pietrasz, J. Yang, R. Soltis, K. Sun, M. Sulek, R. Novak, *ECS Trans.*, 2013, **58,** 1779-1788.
[6]. X.X. Wang, S. Hwang, Y.T. Pan, K. Chen, Y.H. He, S. Karakalos, H.G. Zhang, J.S. Spendelow, D. Su, G. Wu, *Nano. Lett.*, 2018, **18,** 4163-4171.
[7]. M.J.Chen, S. Hwang, J.Z. Li, S. Karakalos, K. Chen, Y.H. He, S. Mukherjee, D. Su, G. Wu, *Nanoscale*, 2018, **10,** 17318-17326.
[8]. X.W. Yu, S.Y. Ye, *J. Power Sources*, 2007, **172,** 145-154.
[9]. A.D. Blasi, C.D. Urso, V. Baglio, V. Antonucci, A.S. Arico, R. Ornelas, F. Matteucci, G. Orozco, D. Beltran, Y. Meas, L.G. Arriaga, *J. Appl. Electrochem*, 2009, **39,** 191-196.
[10]. J.C. Cruz, V. Baglio, S. Siracusano, R. Ornelas, L. Ortiz-Frade, L.G. Arriaga, V. Antonucci, A.S. Arico, *J. Nanoparticle Res.*, 2011, **13,** 1639-1646.
[11]. H.Z. Wang, W.C. Xu, S. Richins, K. Liaw, L.T. Yan, M. Zhou, H.M. Luo, *Electrochim. Acta*, 2019, **296,** 945-953.
[12]. S.V. Devaguptapu, S. Hwang, S. Karakalos, S. Zhao, S. Gupta, D. Su, H. Xu, G. Wu, *ACS Appl. Mater. Interfaces*, 2017, **9,** 44567-44578.
[13]. V. Nallathambi, J.W. Lee, S.P. Kumaraguru, G. Wu, B.N. Popov, *J. Power Sources*, 2008, **183,** 34-42.
[14]. L.P. Zhang, Z.H. Xia, *J. Phys. Chem. C*, 2011, **115,** 11170-11176.
[15]. Y. Cheng, S.P. Jiang, *Pro. Nat. Sci-Mater.*, 2015, **25,** 545-553.
[16]. F.L. Lu, J. Sui, J.M. Su, C. Jin, M. Shen, R.Z. Yang, *J. Power Sources*, 2014, **271,** 55-59.
[17]. H.Y. Zhu, P.F. Zhang, S. Dai, *ACS Catal.*, 2015, **5,** 6370-6385.
[18]. D.B. Meadowcroft, *Nature*, 1970, **226,** 847-848.
[19]. H. Liu, X.F. Ding, L.X. Wang, D. Ding, S.H. Zhang, G.L. Yuan, *Electrochim. Acta*, 2018, **259,** 1004-1010.
[20]. Y.L. Zhu, W. Zhou, J. Yu, Y.B. Chen, M.L. Liu, Z.P. Shao, *Chem. Mater.*, 2016, **28,** 1691-1697.
[21]. S.Y. Bie, Y.Q. Zhu, J.M. Su, C. Jin, S.H. Liu, R.Z. Yang, J. Wu, *J. Mater. Chem. A*, 2015, **3,** 22448-22453.
[22]. A. Costa, M.E.M. Jorge, M.D. Carvalho, A. Gomes, M.I.d.S. Pereria, *J. Solid State Electrochem.*, 2013, **17,** 2311-2318.
[23]. Z.Z. Du, P. Yang, L. Wang, Y.H. Lu, J.B. Goodenough, J. Zhang, D.W. Zhang, *J. Power Sources*, 2014, **265,** 91-96.
[24]. J. Wang, Y. Fu, Y.J. Xu, J. Wu, J.H. Tian, R.Z. Yang, *Int. J. Hydrog. Energy*, 2016, **41,** 8847-8854.
[25]. F.D. Kong, S. Zhang, G.P. Yin, J. Liu, A.X. Ling, *Catal. Lett.* , 2014, **144,** 242-247.
[26]. P.H. Benhangi, A. Alfantazi, E. Gyenge, *Electrochim. Acta*, 2014, **123,** 42-50.
[27]. C. Gong, L. Zhao, S. Li, H.W. Wang, Y.S. Gong, R. Wang, B.B. He, *Electrochim. Acta*, 2017, **281,** 338-347.

[28]. P. Hosseini-Benhangi, M.A. Garcia-Contreras, A. Alfantazi, E.L. Gyenge, *J. Electrochem. Soc*, 2015, **162,** F1356-F1366.
[29]. E. Oakton, D. Lebedev, M. Povia, D.F. Abbott, E. Fabbri, A. Fedorov, M. Nachregaal, C. Coperet, T.J. Schmidt, *ACS Catal.*, 2017, **7,** 2346-2352.
[30]. M. Tariq, W.Q. Zaman, W. Sun, Z.H. Zhou, Y.Y. Wu, L.M. Cao, J. Yang, *ACS Sustainable. Chem. Eng.*, 2018, **6,** 4854-4862.
[31]. L.T. Yan, Y. Lin, W.C. Xu, T. Salas, H. Smalidge, M. Zhou, H.M. Luo, *ACS Appl. Mater. Interfaces*, 2017, **9,** 23820-23827.
[32]. H.Z. Wang, B. Patterson, J.Z. Yang, D. Huang, Y. Qin, H.M. Luo, *Appl. Mater. Today*, 2017, **9,** 402-406.
[33]. C. Jin, X.C. Cao, L.Y. Zhang, C. Zhang, R.Z. Yang, *J. Power Sources*, 2013, **241,** 225-230.
[34]. Y. Xu, L. Fei, E.G. Fu, B. Yuan, J. Hill, Y.X. Chen, S.G. Deng, P. Andersen, Y.Q. Wang, H.M. Luo, *J. Power Sources*, 2013, **242,** 604-609.
[35]. Y.F. Zhu, R.Q. Tan, T. Yi, S.S. Ji, X.Y. Ye, L.L. Cao, *J. Mater. Sci.*, 2000, **35,** 5415-5420.
[36]. M. Soleymani, M. Edrissi, A.M. Alizadeh, *Polymer Journal*, 2015, **47,** 797-801.
[37]. S. He, K.F. Chen, M. Saunders, Z. Quadir, S.W. Tao, J.T.S. Irvine, C.Q. Cui, S.P. Jiang, *Solid State Ion.*, 2018, **325,** 176-188.
[38]. E. Oakton, D. Lebedev, A. Fedorov, F. Krumeich, J. Tillier, O. Sereda, T.J. Schmidt, C. Coperet, *New J. Chem.*, 2016, **40,** 1834-1838.
[39]. R.S. Chen, Y.S. Huang, Y.M. Liang, D.S. Tsai, Y. Chi, J.J. Kai, *J. Mater. Chem.* , 2003, **13,** 2525-2529.
[40]. M. Hara, K. Asami, K. Hashimoto, T. Masumoto, *Electrochim. Acta*, 1983, **28,** 1073-1081.
[41]. P.K. Sonkar, K. Prakash, M. Yadav, V. Ganesan, M. Sankar, R. Gupta, D.K. Yadav, *J. Mater. Chem. A*, 2017, **5,** 6263-6276.
[42]. L.J. Dai, M. Liu, Y. Song, J.J. Liu, F. Wang, *Nano Energy*, 2016, **27,** 185-195.
[43]. J. Shim, K.J. Lopez, H.J. Sun, G. Park, J.C. An, S. Eom, S. Shimpalee, J.W. Weidner, *J. Appl. Electrochem*, 2015, **45,** 1005-1012.
[44]. M.Y. Oh, J.S. Jeon, J.J. Lee, P. Kim, K.S. Naham, *RSC adv.*, 2015, **5,** 19190-19198.
[45]. C.F. Chen, G. King, R.M. Dickerson, P.A. Papin, S. Gupta, W.R. Kellogg, G. Wu, *Nano Energy*, 2015, **13,** 423-432.
[46]. R.A. Rincon, J. Masa, S. Mehrpour, F. Tietz, W. Schuhmann, *Chem. Comm.*, 2014, **50,** 14760-14762.